




# Sustainable Ceramic Membranes from Clays and Mining Wastes by Rapid Sintering Process

Hellen C. T. Firmino<sup>a\*</sup> , Déborah dos S. Gomes<sup>a</sup>, Vanderlane C. da Silva<sup>a,b</sup>, Ieda M. G. Santos<sup>c</sup>,  
Helio L. Lira<sup>a</sup> , Lisiane N. L. Santana<sup>a</sup>, Romualdo R. Menezes<sup>a</sup> , Gelmires de A. Neves<sup>a</sup>

<sup>a</sup>Universidade Federal de Campina Grande, Departamento de Engenharia de Materiais, Laboratório de Tecnologia de Materiais (LTM), 58429-900, Campina Grande, PB, Brasil.

<sup>b</sup>Universidade Federal de Campina Grande, Departamento de Engenharia de Materiais, Programa de Pós-Graduação em Ciência e Engenharia de Materiais, 58429-900, Campina Grande, PB, Brasil.

<sup>c</sup>Universidade Federal da Paraíba, Núcleo de Pesquisa e Extensão - Laboratório de Combustíveis e Materiais (NPE-LACOM), João Pessoa, PB, Brasil.

Received: October 31, 2024; Revised: January 02, 2025; Accepted: January 07, 2025

This study characterized wastes from scheelite and columbite-tantalite mining, as well as kaolin processing, to produce microfiltration membranes for wastewater treatment using a fast-sintered process. After characterization, the wastes were mixed with clays, pressed, and sintered at low temperatures of 1050 and 1100 °C. The resulting membranes exhibited pore size distributions ranging from 3 µm to 180 µm and flexural strengths exceeding 14 MPa. In a crossflow filtration system, permeate fluxes ranged from 177 L/h.m<sup>2</sup> to 228 L/h.m<sup>2</sup> at 2 bar, with permeabilities from 99 to 130 L/h.m<sup>2</sup> bar depending on the waste content. Membranes with smaller pore sizes effectively removed 90% to 96% of turbidity from a water/clay suspension containing micrometric clay particles. This approach demonstrates that rapid sintering of ceramic membranes from mining waste can effectively reduce environmental impacts and energy costs, providing a sustainable solution for wastewater treatment.

**Keywords:** Wastes, scheelite, columbite-tantalite, kaolin, membrane.

## 1. Introduction

Water suitable for human consumption is important for public health, whether for drinking, domestic use, or food production. However, potable water scarcity is a growing global problem that affects around 2.2 billion people, according to the World Health Organization (WHO)<sup>1</sup>. This reduction in the availability of drinking water has been driven by climate change, population growth, and poor water resource management<sup>2</sup>.

Technologies for wastewater reuse, particularly filtration membranes that integrate cost-effectiveness, high efficiency, and ease of operation<sup>3,4</sup>, emerge as promising solutions to address this challenge. These membranes enable the treatment of wastewater, removing pollutants and allowing the water to be used for various purposes. In this context, the use of ceramic membranes produced from mining waste has gained recognition as an environmentally sustainable and cost-effective alternative.

Ceramic membranes act as selective barriers, retaining impurities, including bacteria, viruses, heavy metals, and organic compounds<sup>5-7</sup>. These membranes represent highly effective options for water treatment due to their high mechanical strength and chemical resistance. Such properties render them suitable for use in adverse conditions such as extreme pH, high temperatures, and the presence of aggressive oxidants<sup>8,9</sup>.

Because they have unique properties and a lot of potential uses, minerals like scheelite and columbite-tantalite have been studied a lot when it comes to making ceramics. Scheelite can contain tungsten trioxide concentrations between 0.08–1.5%<sup>10,11</sup>, a metal of great economic importance, with numerous technological applications in sectors such as the metallurgical, electrical, mechanical, aerospace, military, and petroleum industries<sup>12-14</sup>. As a result, scheelite mining activity is intense and profitable, generating a large amount of waste. In this situation, many studies have looked at how to use these mining wastes in ceramic mixtures<sup>15-18</sup>, with the goals of recycling waste and making the created ceramic materials better. Columbite-tantalite is the main source of niobium and tantalum, which are metals that are valued for their ability to conduct electricity, resist corrosion, and be used in high-performance electronic parts<sup>19</sup>. In addition, columbite-tantalite helps make ceramics and glass better by improving their properties like resistance to heat and durability<sup>20</sup>. These minerals and their residues stand out as valuable raw materials for the development of high-performance ceramic materials in various industries.

Several studies have explored the replacement of conventional raw materials commonly used in ceramic membranes with industrial waste for cost reduction and have shown the efficiency of these membranes in removing up to 99% of contaminants<sup>7,21-25</sup>. Kamarudin et al.<sup>21</sup> prepared ceramic hollow fiber membranes composed of metakaolin

\*e-mail: [hellentorrano@hotmail.com](mailto:hellentorrano@hotmail.com)

and corncob ash waste for water filtration and oil-water separation. They showed that the fiber with a ratio of 75:25 (metakaolin:waste) exhibited a permeability of 1359.93 L/m<sup>2</sup>.h and an oil/water removal efficiency of 74.73%. While Rakcho et al.<sup>23</sup> demonstrated the efficiency in the treatment of tannery wastewater and seawater using porous ceramic membranes composed of 20% tea waste and red clay. The membranes exhibited permeability of 1249 L/m<sup>2</sup>.h.bar and achieved turbidity removal efficiencies of 99.76% for seawater and 99.16% for tannery wastewater. Recently, Wang et al.<sup>24</sup> used solid wastes such as coal fly ash, river sediments, and sewage sludge as raw materials to provide an Al-Si-O matrix in single-layer ceramic membranes. These membranes were applied to oily water treatment, achieving oil rejection of over 98% and an oil/water emulsion permeate flux of approximately 1200 L/m<sup>2</sup>.h. In another study, Shiwa et al.<sup>26</sup> incorporated up to 30% of phosphorus slag (PS) and blast furnace slag (BFS) in the composition of mullite-zeolite membranes, obtaining a flux of up to 349 L/m<sup>2</sup>.h and a chemical oxygen demand (COD) removal efficiency of approximately 99% in all evaluated membranes.

On the other hand, other studies have concentrated on thermal treatment to reduce energy consumption during sintering and lower the overall cost of ceramic membranes<sup>27,28</sup>. Conventional sintering processes often require more than two days due to slow heating rates (0.5 °C-2 °C/min), prolonged hold times (1-5 h), and controlled cooling (more than 24 h) to ensure adequate densification and minimize thermal stresses, making this a common procedure in processes that demand strict microstructure control<sup>29</sup>. In contrast, rapid sintering techniques such as spark plasma sintering, microwave heating, and rapid thermal processes based on infrared<sup>30-32</sup>, allow the process to be completed in just a few hours, offering a more efficient alternative in terms of time and energy, as well as showing great potential for the efficient manufacturing of ceramic membranes. Studies<sup>33,34</sup> have shown that a fast sintering process of just three hours is effective in producing silica membranes. Studies<sup>35</sup> demonstrated the efficiency of fast sintering in producing porous diatomite bodies for water purification and wastewater treatment. Other studies<sup>36,37</sup> on ceramic membranes observed that rapid sintering favors a uniform/homogenous porous structure and higher bending compared to conventionally processed materials. However, no studies have evaluated the influence of fast sintering on clay-based or waste-based ceramic membranes, despite its technological potential.

Thus, the use of industrial waste in the formulation of ceramic membranes has been investigated as a promising alternative raw material due to its low cost and the need for sustainable use of natural resources. Moreover, rapid firing cycles have the potential to reduce the energy sintering cost of the ceramic membranes, but this approach is still largely underexplored in this technology. Therefore, this study aims to explore the use of three mining waste materials for the manufacture of ceramic membranes by rapid sintering processes, utilizing the wastes as generated with only granulometric separation and without any additional high-energy processing steps, such as milling. The research examines the influence of different concentrations of the scheelite and the columbite-tantalite mining wastes and the kaolin processing

waste on the microstructure and mechanical properties of porous ceramics produced by fast sintering. In this way, it seeks to contribute to a more comprehensive understanding of sustainable water treatment techniques, promoting the valorization of waste and providing insights into the role of ceramic membranes in mitigating the environmental impacts resulting from mining activities.

## 2. Materials and Methods

### 2.1. Raw materials

The ceramic membranes were produced from natural clays and waste from the mining industry. Ball clay (BC) and red clay (RC) (a plastic red clay) from deposits in the Northeast of Brazil, states of Pernambuco and Paraíba, respectively, were used. Scheelite (SW) and Columbite-tantalite (CTW) exploitation wastes and Kaolin processing (KW) waste were generated as byproducts of mining activities in the state of Rio Grande do Norte, Brazil. As the granulometry of the waste is coarse, before the production of the membranes, the raw materials underwent a sieving process. The materials were sieved through 75 µm sieves for clays and 300 µm sieves for wastes.

### 2.2. Characterizations of raw materials

X-ray diffraction (Shimadzu, XRD-6000, Japan) was performed using CuK $\alpha$  radiation ( $\lambda = 1.54 \text{ \AA}$ ), operated at 40 kV and 30 mA, in the  $2\theta$  angular range of 5-60° and step size of 0.02°. The chemical composition was determined using X-ray fluorescence spectrometry (Shimadzu, EDX-720, Japan). The granulometry of the clays was assessed using laser diffraction (Cilas 1064), whereas the granulometry of the residues was determined through a sieving process.

### 2.3. Membrane preparation

The membranes were prepared by adjusting the amounts of the raw materials according to the chemical composition and XRD patterns of the raw materials. The formulas and their respective nomenclatures are described in Table 1.

The raw materials were mixed with oleic acid (0.5% wt), and then 10% distilled water was added to the formulations. After 24 h, to ensure a homogeneous distribution of moisture, cylindrical ( $\phi = 30 \text{ mm}$  and thickness = 2.6 mm) and rectangular ( $b \times h = 47.9 \times 14.5 \text{ mm}$  and thickness = 5 mm) bodies of test were produced by uniaxial pressing at 46 MPa. The bodies were dried and then fast sintered with a heating rate of 30 °C/min and a dwell time of 20 min: RC formulations at 1050 °C and BC formulations at 1100 °C. The firing cycle parameters, such as heating rate, maximum temperature, and soaking time, were determined after some preliminary tests and a review of the literature on the sintering of ceramic bodies with similar compositions.

### 2.4 Membrane characterization

The sintered membranes were characterized by X-ray diffraction (Shimadzu, XRD-6000, CuK $\alpha$ , Japan) and scanning electron microscopy (SEM, TESCAN). The linear firing shrinkage (%S<sub>f</sub>) was determined by the diameters of the membranes before and after the sintering process. To

**Table 1.** Compositions (wt%) and nomenclatures of the formulations used in the preparation of the membranes.

	Raw materials				Compositions (wt %)			
	RC1	RC2	RC3	RC4	BC1	BC2	BC3	BC4
Ball clay	-	-	-	-	25	15	15	10
Red clay	50	40	30	20	-	-	-	-
Scheelite waste	-	-	-	-	50	50	70	80
Columbite-tantalite waste	50	60	70	80	-	-	-	-
Kaolin waste	-	-	-	-	25	35	15	10

determine the porosities and pore diameters with greater precision, a mercury intrusion porosimetry test was conducted (AutoPore IV 9500 V1.09, Micromeritics Corp).

The flexural strength of the membranes was determined by a three-point flexural test (Shimadzu, Autograph AGX, Japan) with a 5 kN load cell, a distance between the supports of 40 mm, and a loading speed of 0.5 mm/min.

Membrane chemical corrosion resistance was evaluated based on the loss of mass of the membranes at room temperature in acidic HCl solution (pH = 1) and basic NaOH solution (pH = 13) for 7 days.

The water flux and filtration capacity were evaluated using a crossflow filtration system. The filtration test was performed in triplicate; the membranes were tested under pressures of 1, 1.5, and 2 bar, remaining 30 min at each pressure. The permeate was collected at every 5 min and weighed on a balance. The water permeate flux was calculated using Equation 1.

$$J = \frac{V}{At} \quad (1)$$

where  $J$  (L/m<sup>2</sup>.h) is the permeate flux,  $V$  (L) is the permeate volume of the collected water,  $A$  (m<sup>2</sup>) is the membrane surface area, and  $t$  (h) is the collection time.

To investigate the separation efficiency of the membranes, a suspension was prepared using water and sodium bentonite (smectite clay) (50 L: 200 g). The clay had an average particle size of 1.72  $\mu$ m. The permeate flow was collected and weighed every 10 min for 60 min under a pressure of 2 bar. The contaminated water and the permeate were subjected to turbidity analysis using a digital turbidimeter (Hanna, Hi 9870302).

One-way analysis of variance (ANOVA) and the Tukey multiple comparison test were used to determine any statistical difference between the data obtained. Statistical analysis was performed at a significance level of 5% ( $p < 0.05$ ).

### 3. Results and Discussion

#### 3.1. Characterization of raw materials

The XRD patterns of raw materials are shown in Figures 1a-e. Quartz (JCPDS 46-1045), kaolinite (ICSD 78-2110), mica (JCPDS 83-1808), feldspar (JCPDS 84-0710), montmorillonite (JCPDS 13-0135), calcite (JCPDS 72-1937), and black tourmaline (JCPDS 46-1460) were the crystalline phases present in the raw materials.

The chemical compositions of the clays and residues are listed in Table 2. Ball clay and red clay are mainly

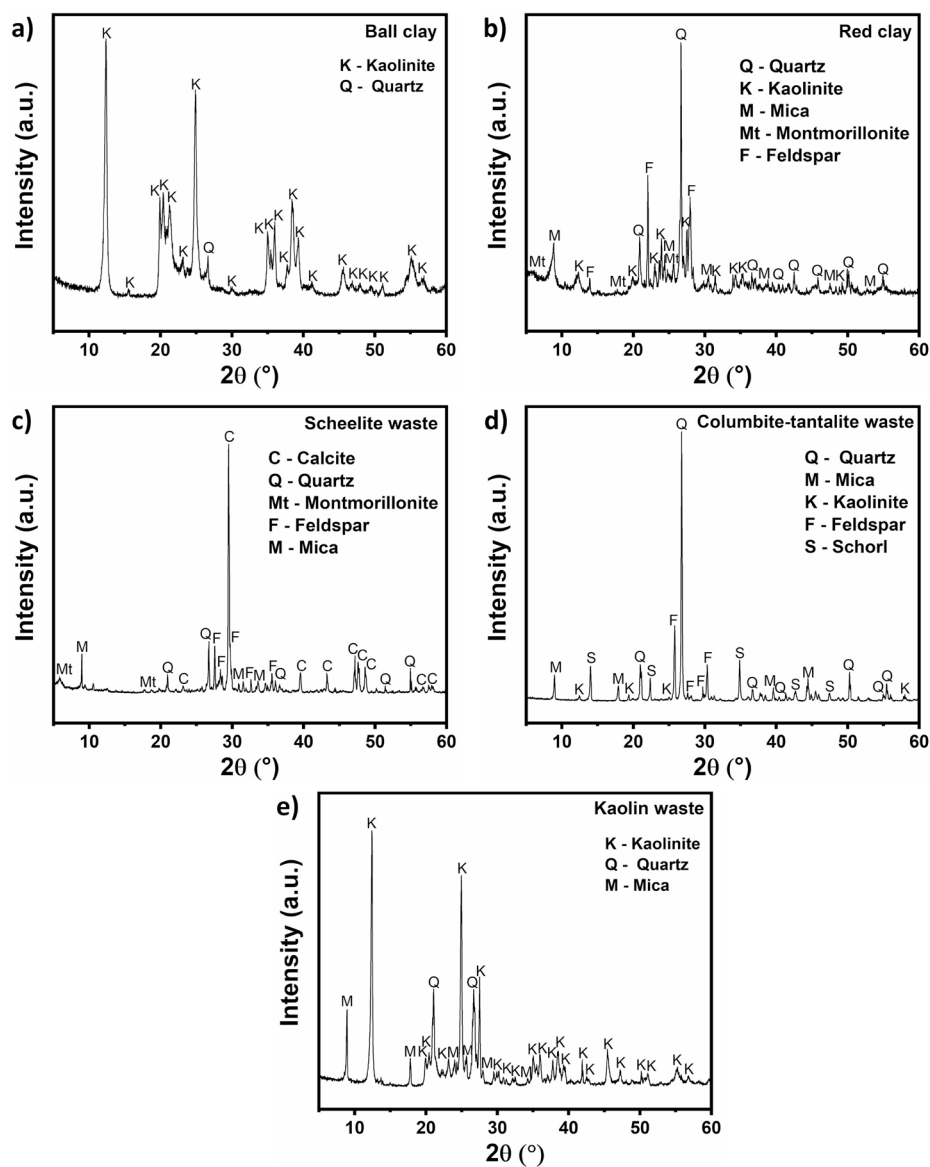
composed of SiO<sub>2</sub> and Al<sub>2</sub>O<sub>3</sub> (SiO<sub>2</sub> + Al<sub>2</sub>O<sub>3</sub> > 79 wt%), due to the presence of clay minerals, quartz, and feldspar<sup>38</sup>. Other oxides such as Fe<sub>2</sub>O<sub>3</sub> (3.2–8.4 wt%), MgO (0.6–3.1 wt%), and K<sub>2</sub>O (0.3–4.6 wt%) were detected in both clays and can act as fluxing oxides. In addition, minor amounts of CaO (2.5 wt%) were identified in the red clay due to the presence of a calcium montmorillonite. Columbite-tantalite and kaolin wastes consisted mainly of SiO<sub>2</sub> (29.9–58.3 wt%) and Al<sub>2</sub>O<sub>3</sub> (11.4–38.8 wt%) but also contained significant amounts of Fe<sub>2</sub>O<sub>3</sub> (1.0–8.5 wt%), MgO (1.1–2.6 wt%), and K<sub>2</sub>O (2.5–5.3 wt%). Scheelite waste is primarily composed of CaO (42.7 wt%), SiO<sub>2</sub> (29.9 wt%), and Al<sub>2</sub>O<sub>3</sub> (11.4 wt%), and it also contains a significant amount of Fe<sub>2</sub>O<sub>3</sub> (8.9 wt%). The high CaO content is associated with the presence of calcite, as evidenced by XRD (Figure 1c). The presence of residual WO<sub>3</sub> is commonly observed in scheelite waste, which aligns with findings reported in the literature<sup>17,25</sup>.

Table 3 summarizes the particle size distribution of the raw materials used. Clays contain particles with dimensions smaller than 20  $\mu$ m and average diameters of 5.13  $\mu$ m for red clay and 2.54  $\mu$ m for ball clay. The D<sub>90</sub> value for red clay is less than 12  $\mu$ m, while for ball clay, it is less than 6  $\mu$ m (see Table 3). On the other hand, the mining wastes are coarser, with particles larger than 100 microns. SW presented a D<sub>50</sub> value below 90  $\mu$ m, while CTW and KW presented a D<sub>50</sub> greater than 150  $\mu$ m (D<sub>50</sub> 200  $\mu$ m and 164  $\mu$ m, respectively).

#### 3.2. Membranes characterizations

Figures 2a-b show the XRD patterns of the membranes after the fast sintering process. The membranes of compositions RC1 to RC4 (Figure 2a) showed characteristic peaks of quartz (JCPDS 46-1045), feldspar (JCPDS 84-0710), and mullite (JCPDS 73-1253). On the other hand, for the membranes of compositions BC1 to BC2 (Figure 2b), peaks of quartz (JCPDS 46-1045), mullite (JCPDS 73-1253), diopside (JCPDS 86-0001), and anorthite (Ca-feldspar, JCPDS 20-0020) were observed. The high contents of CaO and the presence of MgO in scheelite waste (SW) (see Table 2) favored the development of anorthite and diopside phases in the membranes during the sintering process at 1100 °C.

SEM images of the surfaces of membranes of compositions RC1 and BC1 after sintering at 1050 °C and 1100 °C, respectively, are shown in Figures 3a-b. Membranes RC2, RC3, and RC4 exhibited a similar morphology to membrane RC1, while membranes BC2, BC3, and BC4 exhibited a similar morphology to membrane BC1. The surface of the membranes is overall homogeneous, featuring uniformly distributed pores and no presence of cracks.



**Figure 1.** XRD patterns of the raw materials (a) ball clay, (b) red clay and the residues of (c) scheelite, (d) columbite-tantalite and (e) kaolin.

**Table 2.** Chemical composition (wt%) of the raw materials used in this work.

Samples	SiO <sub>2</sub>	Al <sub>2</sub> O <sub>3</sub>	Fe <sub>2</sub> O <sub>3</sub>	CaO	MgO	K <sub>2</sub> O	WO <sub>3</sub>	Other oxides
Ball clay	50.3	44.2	3.2	-	0.6	0.3	-	1.4
Red clay	53.0	26.5	8.4	2.5	3.1	4.6	-	1.9
Scheelite waste	29.9	11.4	8.9	42.7	3.6	-	0.4	3.1
Columbite-tantalite waste	65.0	22.4	5.2	-	1.2	3.4	-	2.8
Kaolin waste	53.7	38.8	1.0	-	1.1	5.3	-	0.1

**Table 3.** Particle size of the clays and residues used to produce the membranes.

	Particle size (µm)				
	Ball clay	Red clay	Scheelite waste	Columbite-tantalite waste	Kaolin waste
D <sub>10</sub>	0.46	0.82	50	115	77
D <sub>50</sub>	2.01	3.88	87	200	164
D <sub>90</sub>	5.47	11.80	179	273	262



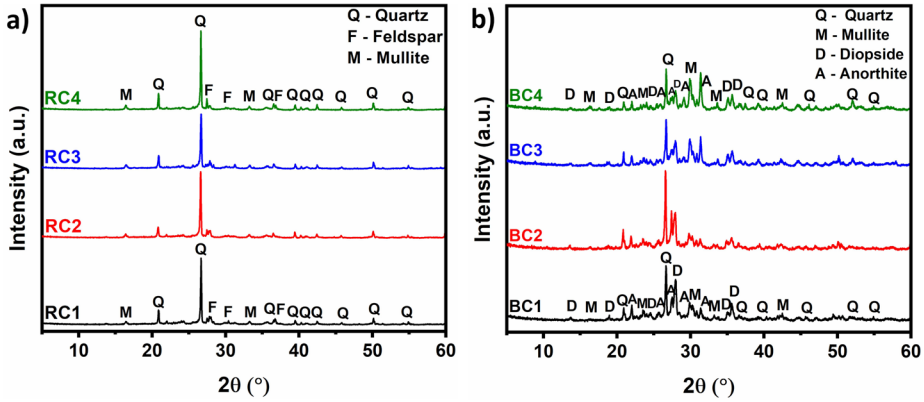


**Figure 2.** XRD patterns of membranes containing (a) RC and CTW after sintering at 1050 °C and (b) BC, SW and KW after sintering at 1100 °C.

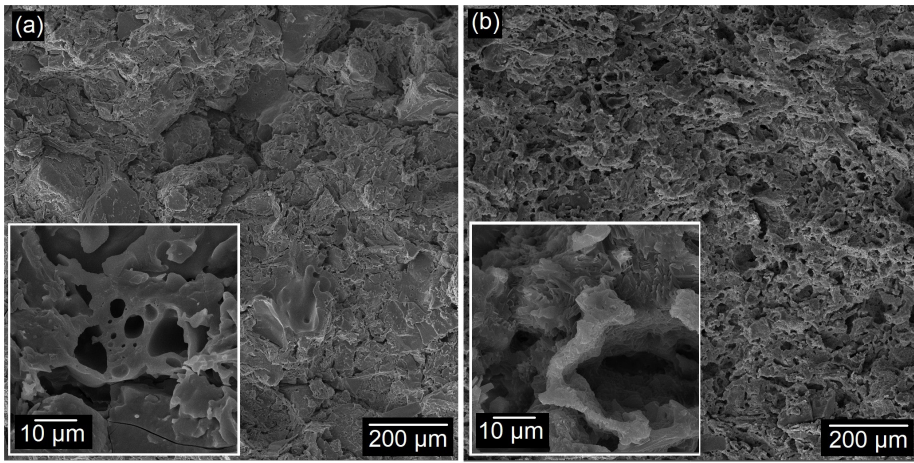


**Figure 3.** SEM images of the surface of the membranes of compositions (a) RC1 obtained at 1050 °C and (b) BC1 obtained at 1100 °C.

The pore size distribution, porosity, and mean pore diameter of the sintered membranes were determined using mercury intrusion porosimetry, and the results are presented in Figures 4a-b and Table 4. The membranes in groups RC1 to RC4 (Figure 4a) exhibited a broader pore size distribution, ranging from 3  $\mu\text{m}$  to over 100  $\mu\text{m}$ . The membranes had a bimodal distribution of pore sizes, with one concentration of pore size between 3 and 10  $\mu\text{m}$  and a volume of pores smaller than 10  $\mu\text{m}$  of around 45%. The curves became wider as the CTW content increased from 50 wt% to 80 wt%, with an increase in the mean pore size and porosity with the amount of CTW. The obtained mean pore diameters were 9  $\mu\text{m}$ , 10  $\mu\text{m}$ , 12  $\mu\text{m}$ , and 15  $\mu\text{m}$  for membranes RC1, RC2, RC3, and RC4, respectively.

On the other hand, for the membranes in groups BC1 to BC4 (Figure 4b), all curves showed a narrow pore size distribution, with pores predominantly between 3  $\mu\text{m}$  and 10  $\mu\text{m}$ . The volume of pores smaller than 10  $\mu\text{m}$  is approximately 80%, highlighting the better packaging behavior of this mass and better interaction of scheelite (SW) and kaolin (KW) residues during sintering. In general, a small broadening in the pore size distributions was observed with the increase of SW from 50 wt% to 80 wt%; however, no change in mean pore size was observed. The porosity increased along with

the increase in the amount of SW up to 70% (70% SW and 15% KW), however, it decreased with the increase in the SW residue to 80% (80% SW and 10% KW). These results showed that an adjustment in the SW/KW ratios was effective in increasing or decreasing porosity, promoting the control of the microstructure of the membranes. SW, predominantly composed of oxides such as CaO and SiO<sub>2</sub>, contributes to the formation of a matrix that promotes partial melting and pore filling during sintering. On the other hand, KW, rich in alumina and silicate, helps stabilize the ceramic structure, reducing the formation of large pores. As the amount of SW increases (50 to 80% by weight), a slight widening in the distribution of pore sizes occurs, but the balance provided by the presence of KW keeps the distribution predominantly narrow, with pores between 3 and 10  $\mu\text{m}$ . All membranes of the group BC1 to BC4 exhibited a mean pore size of 5  $\mu\text{m}$ , which indicates their suitability for microfiltration applications.

Figures 5a-d show the data on firing shrinkage and flexural strength of membranes RC1 to RC4 after sintering at 1050 °C. The differences between the determined values were evaluated using Tukey's comparison test of one-way ANOVA, observing that the increase in CTW content provided a gradual increase in shrinkage ( $p$ -values < 0.05). When the

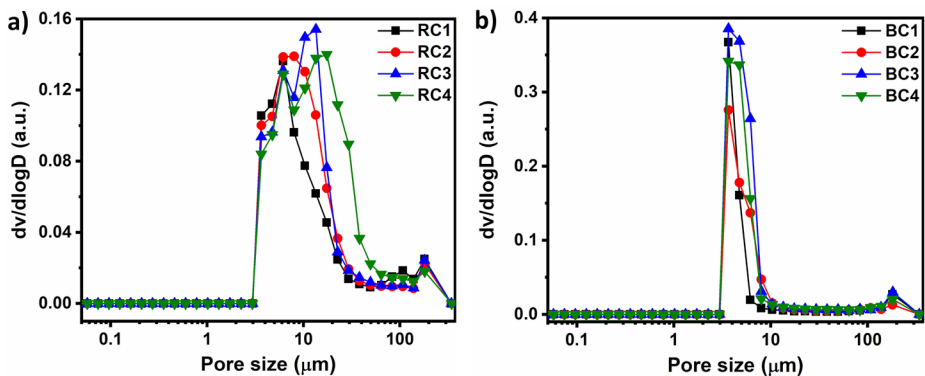


Figure 4. Pore size distribution of the membranes of compositions (a) RC1 to RC4 and of compositions (b) BC1 to BC4.

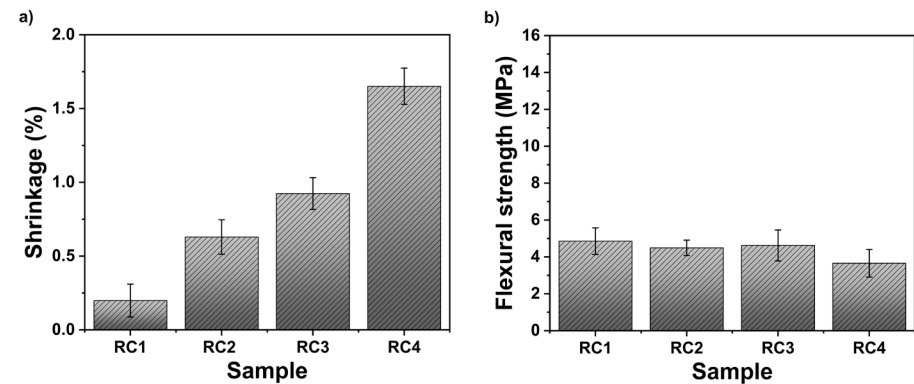


Figure 5. a) Shrinkage and b) flexural strength of membranes in compositions RC1 to RC4.

Table 4. Values of average pore diameters and porosity of sintered membranes obtained by mercury intrusion porosimetry.

	Sample							
	RC1	RC2	RC3	RC4	BC1	BC2	BC3	BC4
Average pore diameter ( $\mu m$ )	9	10	12	15	5	5	5	5
Porosity (%)	18	21	22	25	14	15	24	19

amount of residue increased from 50 wt% (RC1 sample) to 80 wt% (RC4 sample), there was an increase in shrinkage from 0.2% to 1.7% between these samples, indicating that CTW slowed down the densification process. On the other hand, no statistically significant differences were observed in the flexural strength of the membranes ( $p$ -values  $> 0.05$ ), despite the increase in CTW content. The flexural strength values remained constant, indicating that the incorporation of CTW did not affect the mechanical integrity of the membranes under the conditions tested.

Figures 6a-b show the shrinkage and flexural strength data for the BC1 to BC4 membranes sintered at 1100 °C. Increasing the SW content from 50 wt% (BC1 sample) to 80 wt% (BC4 sample), along with a reduction in KW and BC content, led to a decrease in shrinkage, from 0.4% to an expansion of -0.3% ( $p$ -values  $< 0.05$ ). This behavior can be attributed to the presence of calcite in SW (see Figure 1c), as calcite acts as a carbonate source and releases CO<sub>2</sub> during sintering<sup>39</sup>. The release of CO<sub>2</sub> caused the expansion phenomenon observed in the BC4 membrane<sup>40</sup>, which had the highest SW content. However, BC1 and BC2 membranes

did not exhibit statistically significant differences in the parameters evaluated ( $p$ -value = 0.210), suggesting that SW content below a certain threshold does not significantly affect the material's shrinkage or expansion.

Statistical analysis indicated that there was no significant difference in flexural strength between the BC1 and BC2 membranes ( $p$ -value = 0.940), as well as between BC3 and BC4 ( $p$ -value = 0.650). However, an increase in flexural strength from 9.5 MPa to 13.5 MPa was observed when the SW content increased from 50 wt.% (BC1 sample) to 80 wt.% (BC4 sample) ( $p$ -value = 0.0003), indicating that the higher SW content positively contributed to strengthening the membranes. This behavior can be explained by the presence of anorthite and diopside phases (see Figure 2b), which contribute to an improvement in flexural strength<sup>41,42</sup>. The presence of anorthite enhances the strength of the bodies by forming a microcomposite microstructure with the aluminosilicate phases in the body<sup>43,44</sup>. Previous studies<sup>45,46</sup> have also reported that the flexural strength of the crystalline phases anorthite and diopside is correlated with their respective crystalline structures. The presence of these crystalline phases hinders

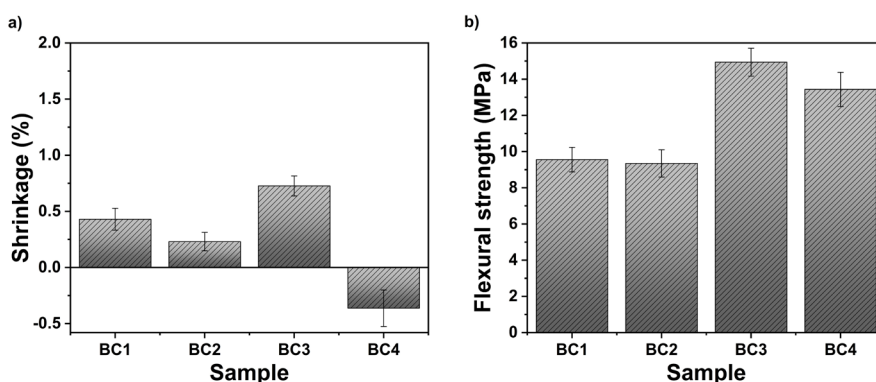


Figure 6. a) shrinkage and b) flexural strength of membranes in compositions BC1 to BC4.

dislocation movement and crack propagation, resulting in enhanced flexural strength. Therefore, the simultaneous presence of anorthite and diopside, along with the nucleation and growth of mullite, which is undoubtedly one of the most important phases for achieving mechanical strength in ceramic materials<sup>47</sup>, resulted in an increase in the strength of the BC1 to BC4 membranes compared to the RC1 to RC4 membranes (see Figure 5b).

The membranes produced in this study exhibited flexural strength superior to those reported by Lima et al.<sup>47</sup>, Manni et al.<sup>48</sup> and Mohamed et al.<sup>49</sup>, while using the same sintering temperature. This was achieved with a single, rapid heating ramp, resulting in membranes free of defects such as cracks or deformations. Manni et al.<sup>48</sup> manufactured membranes from Moroccan natural magnesite using two heating ramps: the first up to 500 °C at 2 °C/min for 2 hours, followed by a second ramp to 1100 °C at the same rate for another 2 hours. The authors stated that this firing schedule was designed to minimize defects such as cracks and deformations, yielding a flexural strength of approximately 6 MPa. Similarly, Mohamed et al.<sup>49</sup> produced membranes from Cameroonian clay, bovine bone ash, and cassava starch, also using two heating ramps. The first ramp reached 700 °C at 2 °C/min, and the second reached 1100 °C at 5 °C/min for 2 hours, resulting in a maximum flexural strength of 5 MPa. More recently, Lima et al.<sup>47</sup> fabricated kaolin and alumina membranes with two heating ramps to eliminate organic matter used as a pore-forming agent. The first ramp reached 500 °C at 5 °C/min for 1 hour, followed by the second ramp to 1100 °C with the same rate and dwell time, achieving a flexural strength of 11 MPa. Therefore, the single, rapid heating cycle used in this study not only simplified the process but also led to superior flexural strength without compromising the structural integrity of the membranes.

Table 5 shows the results of the corrosion test of the membranes after 7 days of immersion in acidic and basic environments. Membranes RC1 to RC4 showed high stability in both environments, with mass losses limited to 0.5% in an acidic environment and 1.0% in a basic environment, demonstrating good corrosion resistance. On the other hand, membranes BC1 to BC4 showed negligible mass variations in a basic environment, but in an acidic environment, they recorded significant loss of mass, reaching up to 11%. This

susceptibility to corrosion in alkaline solutions is due to the presence of the diopside and anorthite phases, which are related to their calcium-rich composition and silicate structure, which favor dissolution in acidic media<sup>50</sup>. These results indicate that all the produced membranes can maintain their functional properties over time in a basic environment, but only the RC group exhibits stability under acidic conditions. Membranes with greater corrosion resistance reduce the need for frequent replacements, particularly in the treatment of industrial effluents or wastewater, thereby making the process more economical and sustainable. Thus, for industrial effluents, the RC group appears to be the most stable membrane. However, in the treatment of potable water, where pH conditions typically range from 6.5 to 7.5, the requirements for the membranes are reduced.

### 3.3. Membrane performance evaluation

The permeability of the membranes was evaluated using distilled water, and the results are shown in Figures 7a-b and Table 6. The increase in pressure significantly enhanced the permeate water flux through the membranes, which is in agreement with the principles described by Darcy's Law<sup>51</sup>. The permeate fluxes obtained at 2 bar were 185 L/h.m<sup>2</sup>, 200 L/h.m<sup>2</sup>, 206 L/h.m<sup>2</sup> and 228 L/h.m<sup>2</sup> for the membranes of compositions RC1, RC2, RC3, and RC4, respectively. For the membranes of compositions BC1, BC2, BC3, and BC4, the permeate fluxes achieved at 2 bar were 177 L/h.m<sup>2</sup>, 183 L/h.m<sup>2</sup>, 225 L/h.m<sup>2</sup> and 189 L/h.m<sup>2</sup>, respectively. The results indicate that the flux in ceramic membranes is directly related to their porosity. Membranes that presented higher porosity, such as RC4 and BC3, also exhibited higher permeate fluxes.

Flow results obtained using distilled water alone do not allow for an accurate comparison of the performance of two or more membranes when tests are conducted under different pressures. In this context, permeability becomes a more appropriate metric for comparing membrane performance regardless of the applied pressure. For example, Lagdali et al.<sup>52</sup> produced microfiltration membranes using clay as raw materials, firing at different temperatures with slow heating rates and longer sintering times. These membranes exhibited a maximum flux of 8.52 L/h.m<sup>2</sup> with distilled water and a permeability of 43.50 L/h.m<sup>2</sup>.bar. Similarly,

**Table 5.** Loss of mass after 7 days of corrosion testing in acidic and basic environments.

Condition	Loss of mass (wt%)							
	RC1	RC2	RC3	RC4	BC1	BC2	BC3	BC4
Acidic pH	0.4	0.3	0.3	0.5	8.8	10.2	6.9	11.0
Basic pH	1.0	0.8	1.0	1.0	-0.1	0.3	-0.3	-0.5

**Table 6.** Membranes permeability.

Permeability (L/h.m <sup>2</sup> .bar)							
RC1	RC2	RC3	RC4	BC1	BC2	BC3	BC4
100	114	121	130	99	103	123	107

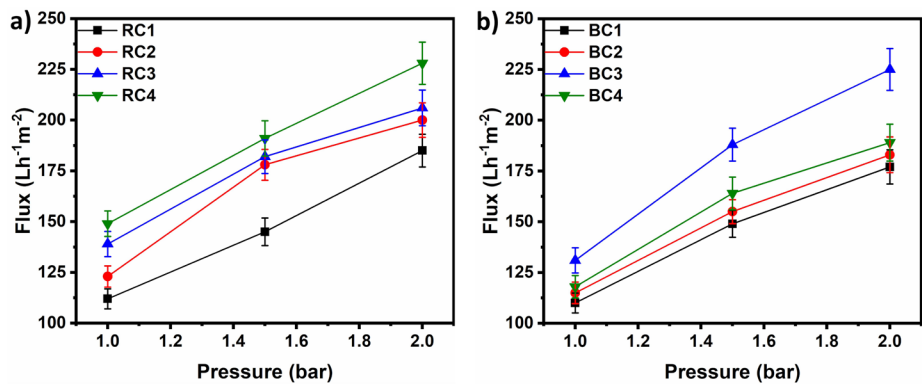


**Figure 7.** Evolution of permeate water flux as a function of pressure for membranes with compositions (a) RC1 to RC4 and for membranes with compositions (b) BC1 to BC4. Feed: distilled water.

Alsubei et al.<sup>53</sup> produced microfiltration membranes using white clay, ground silica, gum arabic, and marble powder, also employing extended sintering times. These membranes demonstrated a maximum flux of 116 L/h.m<sup>2</sup> with distilled water, with permeability ranging between 67 and 156 L/h.m<sup>2</sup>.bar. The flux values obtained in this study surpass those reported by Lagdali et al.<sup>52</sup> and Alsubei et al.<sup>53</sup>, while the permeability is higher than Lagdali et al.<sup>52</sup> and comparable to Alsubei et al.<sup>53</sup>, highlighting the efficiency of the membranes developed in this work.

Membranes with compositions RC1 to RC4 and BC1 to BC4 were evaluated for filtration performance using a feed solution prepared from tap water and sodium bentonite at a transmembrane pressure of 2 bar. The performance of the membranes was analyzed in terms of permeate flux (Figures 8a-b) and turbidity reduction (Figures 9a-b). The permeate flux gradually increased with the amount of CTW for membranes RC1 to RC4 (Figure 8a). The permeate flux followed the order: RC4 (9.1 L/h.m<sup>2</sup>) > RC3 (5 L/h.m<sup>2</sup>) > RC1 (3.0 L/h.m<sup>2</sup>) > RC2 (2.7 L/h.m<sup>2</sup>). This is likely due to the higher porosity of RC4 (25%) compared to the lower porosity of membranes RC1 to RC3. For membranes with compositions BC1 to BC4 (Figure 8b), the permeate flux followed the order: BC4 (5.2 L/h.m<sup>2</sup>) > BC2 (4.9 L/h.m<sup>2</sup>) > BC3 (4.3 L/h.m<sup>2</sup>) > BC1 (3.9 L/h.m<sup>2</sup>). This also indicates that the higher amount of SW in the BC4 membrane allowed porosity and pore distribution that resulted in higher flux. However, flux values may also be affected by tortuosity and pore connectivity<sup>54</sup>, requiring further investigation.

Figures 9a-b illustrate the turbidity analysis results following the filtration process. The initial suspension turbidity

was 18 NTU, with an average clay particle size of 1.72 µm. According to the World Health Organization (WHO), the maximum permissible turbidity value for drinking water is 5 NTU<sup>55</sup>. All membranes, except for the RC4 membrane, demonstrated satisfactory performance. The unsatisfactory performance of the RC4 membrane may be attributed to its high porosity and larger average pore diameter and pore size distribution, which can reduce the retention capacity for clay particles, resulting in higher permeate flux but lower filtration efficiency. Membranes with compositions RC1, BC2, BC3, and BC4 exhibited the lowest turbidity levels, with removal rates of 90% (1.8 NTU), 96% (0.68 NTU), 91% (1.6 NTU), and 90.5% (1.7 NTU), respectively. This behavior can be attributed to smaller pore sizes and a more suitable pore size distribution, which prevent particle passage, highlighting the efficiency of the produced membranes in retaining particles for microfiltration applications. Lagdali et al.<sup>52</sup> evaluated the efficiency of microfiltration on real pre-treated wastewater from a laundry in Morocco, and Alsubei et al.<sup>53</sup> used tap water with bentonite clay. Both studies achieved similar flux rates and removal values to this work.

Table 7 presents a comparison between the membranes produced in this study and those reported in other studies published in international journals. The membranes developed in this study are predominantly composed of waste materials that would otherwise be discarded into the environment. Additionally, these membranes were sintered in a single step, contributing to energy savings in the process.

The results demonstrated that the distilled water permeability of the produced membranes was superior, while their efficiency in contaminant removal was similar to or close to the values



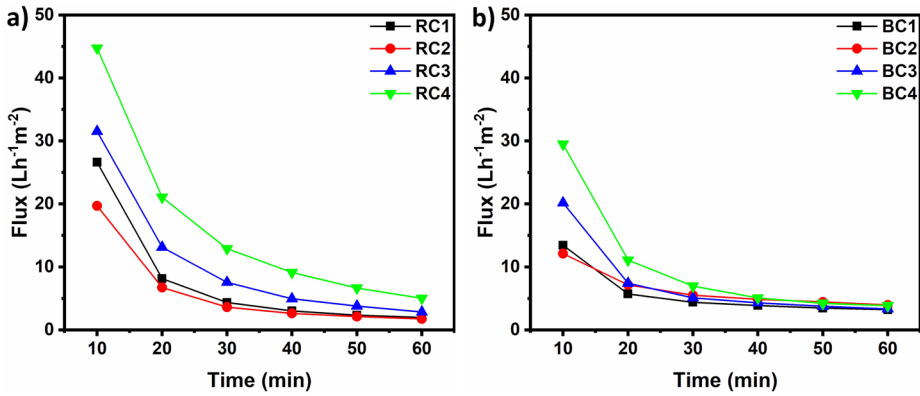


**Figure 8.** Permeate water flux as a function of time for membranes with compositions (a) RC1 to RC4 and for membranes with compositions (b) BC1 to BC4. Feed solution: Tap water and bentonite clay.

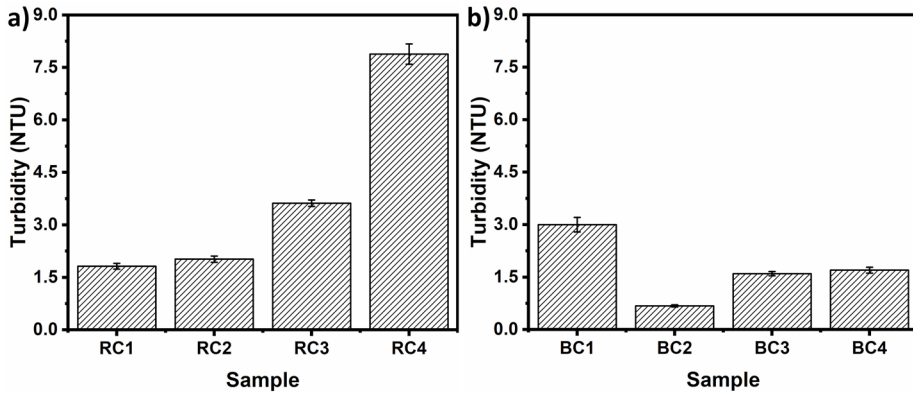


**Figure 9.** Turbidity reduction efficiency of membranes with compositions (a) RC1 to RC4 and compositions (b) BC1 to BC4. Feed solution: Tap water and bentonite clay.

**Table 7.** Comparison between the membranes produced in this study and membranes reported in other studies.

Material	Sintering	Permeability distilled water	Contaminant removal	Contaminant/particle size	Reference
Phengite clay	1 - 250 °C	43.5 L/h.m <sup>2</sup> .bar	100%	Real wastewater/ 100 µm mesh	52
	2 °C/min				
	60 min				
	2 -1050 °C				
White clay	5 °C/min	67 L/h.m <sup>2</sup> .bar	99.2%	Bentonite clay 1.1 µm	53
	120 min				
	1 - 100 °C				
	2 °C/min				
Silica flour	60 min	100-130 L/h.m <sup>2</sup> .bar	1.82%-7.88%	Clay/1.72 µm	This work
	2 - 500 °C				
	5 °C/min				
	60 min				
Arabic gum	3 - 1200 °C	99-123 L/h.m <sup>2</sup> .bar	83%-96%	Clay/1.72 µm	This work
	5 °C/min				
	60 min				
	1 - 1050 °C				
Red clay	30 °C/min	99-123 L/h.m <sup>2</sup> .bar	83%-96%	Clay/1.72 µm	This work
Columbite-tantalite waste	20 min				
Ball-clay	1 - 1100 °C	99-123 L/h.m <sup>2</sup> .bar	83%-96%	Clay/1.72 µm	This work
Scheelite waste	30°C/min				
Kaolin waste	20 min				

reported in comparative studies. Furthermore, the size of the retained contaminant particles was smaller or comparable to those described in other studies, highlighting the efficacy of the membranes in retaining micrometric particles (up to approximately 1.7  $\mu\text{m}$ ).

Therefore, in addition to contributing to water recovery, membranes produced through fast-burn cycles offer significant potential for reducing sintering costs. This method also increases environmental sustainability, making it a promising solution for large-scale production, particularly in industries that aim to reduce energy consumption and manufacturing costs.

## 4. Conclusion

Microfiltration ceramic membranes composed mainly of mining industry waste were manufactured using rapid sintering, highlighting the potential of mining-wastes as raw materials for ceramic materials and the rapid firing technique. The produced membranes presented average pore diameters ranging from 5  $\mu\text{m}$  to 15  $\mu\text{m}$ , according to the composition. An increase in waste content did not result in statistically significant variations in the flexural strength of the red clay-based membranes, while the ball clay-based membranes led to a 40% increase in mechanical strength. Produced membranes presented high chemical resistance in both acidic environments and permeate flux, which ranged from 177 L/h.m<sup>2</sup> to 228 L/h.m<sup>2</sup> under a pressure of 2 bar. The membranes with smaller pores achieved up to 96% particle turbidity removal. These results underscore the feasibility and sustainability of utilizing industrial waste in ceramic membrane production, contributing to environmental preservation by reducing the need for unused natural resources, and highlight the efficiency of the rapid firing cycle in the fabrication of ceramic membranes, which has high potential for reducing the sintering cost of the production of these membranes.

## 5. Acknowledgments

The authors would like to thank the Brazilian research funding agency CNPq (National Council for Science and Technology), grant nos. 405364/2021-0 e 407848/2022-3, 309771/2021-8, 405364/2021-0 and 407848/2022-3; CAPES (Coordenação de Aperfeiçoamento de Pessoal de Nível Superior), Finance Code 001 (scholarships granted Vanderlane Cavalcanti da Silva); and FINEP (Notice Advanced Materials, term 0052/21) for their financial support.

## 6. References

- WHO: World Health Organization. The measurement and monitoring of water supply, sanitation and hygiene (WASH) affordability: a missing element of monitoring of sustainable development goal (SDG) targets 6.1 and 6.2. Geneva: WHO; 2021.
- Liu R, Chen Q, Cao M, Lin J, Lin F, Ye W, et al. Robust bio-inspired superhydrophilic and underwater superoleophobic membranes for simultaneously fast water and oil recovery. *J Membr Sci.* 2021;623:119041. <http://doi.org/10.1016/j.memsci.2020.119041>.
- Zhao S, Shen L. Advanced membrane science and technology for sustainable environmental applications. *Front Chem.* 2020;8:609774.
- Ye W, Liu R, Chen X, Chen Q, Lin J, Lin X, et al. Loose nanofiltration-based electrodialysis for highly efficient textile wastewater treatment. *J Membr Sci.* 2020;608:118182. <http://doi.org/10.1016/j.memsci.2020.118182>.
- Zuo K, Wang K, DuChanois RM, Fang Q, Deemer EM, Huang X, et al. Selective membranes in water and wastewater treatment: role of advanced materials. *Mater Today.* 2021;50:516-32. <http://doi.org/10.1016/j.mattod.2021.06.013>.
- Jiang D, Gao C, Liu L, Yu T, Li Y, Wang H. Application of nanoporous ceramic membrane derived from Fe/S/Si/Al/O-rich mining solid waste in oil-water separation and heavy metal removal of industrial high concentrated emulsifying wastewater. *Separ Purif Tech.* 2022;295:121317. <http://doi.org/10.1016/j.seppur.2022.121317>.
- Mouratib R, Achiou B, El Krati M, Younsi SA, Tahiri S. Low-cost ceramic membrane made from alumina-and silica-rich water treatment sludge and its application to wastewater filtration. *J Eur Ceram Soc.* 2020;40(15):5942-50. <http://doi.org/10.1016/j.jeurceramsoc.2020.07.050>.
- Rani SLS, Kumar RV. Insights on applications of low-cost ceramic membranes in wastewater treatment: a mini-review. *Case Stud Chem Environ Eng.* 2021;4:100149. <http://doi.org/10.1016/j.csee.2021.100149>.
- Yue M, Zhao S, Feron PH, Qi H. Multichannel tubular ceramic membrane for water and heat recovery from waste gas streams. *Ind Eng Chem Res.* 2016;55(9):2615-22. <http://doi.org/10.1021/acs.iecr.6b00242>.
- Hällström LP, Alakangas L, Martinsson O. Scheelite weathering and tungsten (W) mobility in historical oxidic-sulfidic skarn tailings at Yxsjöberg, Sweden. *Environ Sci Pollut Res Int.* 2020;27(6):6180-92. <http://doi.org/10.1007/s11356-019-07305-1>.
- Leal-Ayala DR, Allwood JM, Petavratzi E, Brown TJ, Gunn G. Mapping the global flow of tungsten to identify key material efficiency and supply security opportunities. *Resour Conserv Recycling.* 2015;103:19-28. <http://doi.org/10.1016/j.resconrec.2015.07.003>.
- Souza GM, Amorim EF, Anjos MAS, França FAN. Estudo de misturas compostas por resíduos de scheelita e solos destinados a pavimentação. *Ambient Constr.* 2023;23(3):117-37. <http://doi.org/10.1590/s1678-86212023000300679>.
- Vemuri R, Engelhard MH, Ramana C. Correlation between surface chemistry, density, and band gap in nanocrystalline WO<sub>3</sub> thin films. *ACS Appl Mater Interfaces.* 2012;4(3):1371-7. <http://doi.org/10.1021/am2016409>.
- Leffler PE, Kazantzis GT. Tungsten. In: Nordberg GF, Fowler BA, Nordberg M, editors. *Handbook on the toxicology of metals.* Amsterdam: Elsevier; 2015. p. 1297-306. <http://doi.org/10.1016/B978-0-444-59453-2.00058-5>.
- Souza M, Neta M, Barros S, Dantas G, Neves G, Cartaxo J, et al. Influência do tipo de cura no comportamento mecânico de argamassas confeccionadas com areia de scheelita. *Rev Eletrôn Mater e Process.* 2019;14(2):91-4.
- Medeiros PSS, Lucena Lira H, Rodriguez MA, Menezes RR, Araújo Neves G, Lima Santana LN. Incorporation of quartzite waste in mixtures used to prepare sanitary ware. *J Mater Res Technol.* 2019;8(2):2148-56. <http://doi.org/10.1016/j.jmrt.2019.02.001>.
- Medeiros B, Neves G, Barbosa N, Menezes R, Ferreira H. Mechanical properties of mortar produced with the replacement of natural sand by scheelite residue. *Ceramica.* 2019;65(375):443-51. <http://doi.org/10.1590/0366-69132019653752571>.
- Figueirêdo JMR, Costa FP, Fernandes JV, Rodrigues AM, Neves GA, Menezes RR, et al. Development of scheelite tailings-based ceramic formulations with the potential to manufacture porcelain tiles, semi-stoneware and stoneware. *Materials.* 2020;13(22):5122. <http://doi.org/10.3390/ma13225122>.
- Franco JA, Cramer T, Bonilla A, Castañeda AJ, Poujol M, Amaya Z. Mineralogía y geocronología de rutilo-(Nb, Ta)

- relacionado a casiterita y columbita-tantalita provenientes de rocas Mesoproterozoicas del Cratón Amazónico cerca de Cachicamo, Colombia. *Bol Geo*. 2021;43(1):99-126.
20. Castro GA, Díaz AA. Estudio de un mineral de columbo-tantalita con enfoque metalúrgico para definir el aprovechamiento de depósitos de arena con minerales pesados. *Av Cienc Ing*. 2016;7(2):9-16.
  21. Kamarudin NH, Harun Z, Othman MHD, Abdullahi T, Bahri SS, Kamarudin NH, et al. Waste environmental sources of metakaolin and corn cob ash for preparation and characterisation of green ceramic hollow fibre membrane (h-MCa) for oil-water separation. *Ceram Int*. 2020;46(2):1512-25. <http://doi.org/10.1016/j.ceramint.2019.09.118>.
  22. Abd Aziz MH, Othman MHD, Hashim NA, Rahman MA, Jaafar J, Hubadillah SK, et al. Pretreated aluminium dross waste as a source of inexpensive alumina-spinel composite ceramic hollow fibre membrane for pretreatment of oily saline produced water. *Ceram Int*. 2019;45(2):2069-78. <http://doi.org/10.1016/j.ceramint.2018.10.110>.
  23. Rakcho Y, Mouiya M, Bouazizi A, Aboulitiam Y, Sehaqui H, Mansouri S, et al. Treatment of seawater and wastewater using a novel low-cost ceramic membrane fabricated with red clay and tea waste. *Arab J Chem*. 2023;16(11):105277. <http://doi.org/10.1016/j.arabjc.2023.105277>.
  24. Wang Z, Xu Z, Qiu D, Chu Y, Tang Y. Beneficial utilization of Al/Si/O-rich solid wastes for environment-oriented ceramic membranes. *J Hazard Mater*. 2021;401:123427. <http://doi.org/10.1016/j.jhazmat.2020.123427>.
  25. Almeida E, Carreiro M, Rodrigues A, Ferreira H, Santana L, Menezes R, et al. A new eco-friendly mass formulation based on industrial mining residues for the manufacture of ceramic tiles. *Ceram Int*. 2021;47(8):11340-8. <http://doi.org/10.1016/j.ceramint.2020.12.260>.
  26. Shiwa S, Khosravi A, Abbasi M, Mohammadi F, Sillanpää M. Fabrication and characterization of ceramic tubular composite membranes using slag waste materials for oily wastewater treatment. *J Environ Manage*. 2024;367:122065. <http://doi.org/10.1016/j.jenvman.2024.122065>.
  27. Zou D, Fan Y. State-of-the-art developments in fabricating ceramic membranes with low energy consumption. *Ceram Int*. 2021;47(11):14966-87. <http://doi.org/10.1016/j.ceramint.2021.02.195>.
  28. Liu Q, Guo S, Leng S, Zhang H, Cao Z. Preparation and property of porous calcium silicate ceramic by two-step ultrafast high-temperature sintering. *Int J Appl Ceram Technol*. 2024;21(5):3346-54. <http://doi.org/10.1111/ijac.14803>.
  29. Schillo M, Park I-S, Chiu W, Verweij H. Rapid thermal processing of inorganic membranes. *J Membr Sci*. 2010;362(1-2):127-33. <http://doi.org/10.1016/j.memsci.2010.06.030>.
  30. Yoo WC, Stoeger JA, Lee PS, Tsapatsis M, Stein A. High-performance randomly oriented zeolite membranes using brittle seeds and rapid thermal processing. *Angew Chem Int Ed*. 2010;49(46):8699-703. <http://doi.org/10.1002/anie.201004029>.
  31. Gottesman R, Song A, Levine I, Krause M, Islam AN, Abou-Ras D, et al. Pure  $\text{CuBi}_2\text{O}_4$  photoelectrodes with increased stability by rapid thermal processing of  $\text{Bi}_2\text{O}_3/\text{CuO}$  grown by pulsed laser deposition. *Adv Funct Mater*. 2020;30(21):1910832. <http://doi.org/10.1002/adfm.201910832>.
  32. Song H, Wei Y, Qi H. Tailoring pore structures to improve the permselectivity of organosilica membranes by tuning calcination parameters. *J Mater Chem A Mater Energy Sustain*. 2017;5(47):24657-66. <http://doi.org/10.1039/C7TA07117E>.
  33. Wang S, Wang DK, Smart S, Costa JCD. Improved stability of ethyl silicate interlayer-free membranes by the rapid thermal processing (RTP) for desalination. *Desalination*. 2017;402:25-32. <http://doi.org/10.1016/j.desal.2016.09.025>.
  34. Wang DK, Costa JCD, Smart S. Development of rapid thermal processing of tubular cobalt oxide silica membranes for gas separations. *J Membr Sci*. 2014;456:192-201. <http://doi.org/10.1016/j.memsci.2014.01.014>.
  35. Akhtar F, Vasiliev PO, Bergström L. Hierarchically porous ceramics from diatomite powders by pulsed current processing. *J Am Ceram Soc*. 2009;92(2):338-43. <http://doi.org/10.1111/j.1551-2916.2008.02882.x>.
  36. Li Z, Pan W. Preparation and characterization of nanoporous alumina as ceramic membrane materials. *IOP Conf Series Mater Sci Eng*. 2019;678(1):012031. <http://doi.org/10.1088/1757-899X/678/1/012031>.
  37. Alves PCF, Silva DG, Vasconcelos DCL, Vasconcelos W, Nascimento JF, Melo DC, et al. Influence of sintering parameters on the structure of alumina tubular membranes obtained by freeze-casting. *J Ceram Sci Technol*. 2023;14(2):89-98.
  38. Fernandes JV, Guedes DG, da Costa FP, Rodrigues AM, Neves GA, Menezes RR, et al. Sustainable ceramic materials manufactured from ceramic formulations containing quartzite and scheelite tailings. *Sustainability*. 2020;12(22):9417. <http://doi.org/10.3390/su12229417>.
  39. Khedidja M, Bechir M, Feyda S, Ali TM. Development of ceramic filtering membranes based on Tunisian clay and phosphate sludge in wastewater treatment. *Solid State Sci*. 2024;148:107430. <http://doi.org/10.1016/j.solidstatesciences.2023.107430>.
  40. Martínez JD, Betancourt-Parra S, Carvajal-Marín I, Betancur-Vélez M. Ceramic light-weight aggregates production from petrochemical wastes and carbonates ( $\text{NaHCO}_3$  and  $\text{CaCO}_3$ ) as expansion agents. *Constr Build Mater*. 2018;180:124-33. <http://doi.org/10.1016/j.conbuildmat.2018.05.281>.
  41. Hosseiny AHM, Najafi A, Khalaj G. Investigation of CaO/MgO on the formation of Anorthite, Diopside, Wollastonite and Gehlenite phases in the fabrication of fast firing ceramic tiles. *Constr Build Mater*. 2023;394:132022. <http://doi.org/10.1016/j.conbuildmat.2023.132022>.
  42. Wu J, Yu J, Xu X, Liu Y, Zhang Z, Wei P. Preparation and thermal shock resistance of anorthite solar thermal energy storage ceramics from magnesium slag. *Ceram Int*. 2022;48(22):33604-14. <http://doi.org/10.1016/j.ceramint.2022.07.305>.
  43. Wang S, Li X, Wang C, Bai M, Zhou X, Zhang X, et al. Anorthite-based transparent glass-ceramic glaze for ceramic tiles: preparation and crystallization mechanism. *J Eur Ceram Soc*. 2022;42(3):1132-40. <http://doi.org/10.1016/j.jeurceramsoc.2021.11.036>.
  44. Traoré K, Kabre TS, Blanchart P. Gehlenite and anorthite crystallisation from kaolinite and calcite mix. *Ceram Int*. 2003;29(4):377-83. [http://doi.org/10.1016/S0272-8842\(02\)00148-7](http://doi.org/10.1016/S0272-8842(02)00148-7).
  45. Kim J, Hwang S, Sung W, Kim H. Effect of anorthite and diopside on dielectric properties of  $\text{Al}_2\text{O}_3$ /glass composite based on high strength of LTCC substrate. *J Mater Sci*. 2008;43(12):4009-15. <http://doi.org/10.1007/s10853-007-2231-4>.
  46. Chen T, Peng T, Sun H, Ding W, Chu L, Wu M, et al. Effect of  $\text{SiO}_2/\text{MgO}$  ratio on the properties of diopside-based ceramics. *Constr Build Mater*. 2024;438:137085. <http://doi.org/10.1016/j.conbuildmat.2024.137085>.
  47. Lima LK, Santana LN, Lira HL, Rodríguez MA, Souza MY, Ribeiro MG Jr, et al. Development of asymmetric ceramic membranes for dairy wastewater treatment: a comparison between co-sintering and conventional firing process. *J Water Process Eng*. 2024;57:104611. <http://doi.org/10.1016/j.jwpe.2023.104611>.
  48. Manni A, Achiou B, Karim A, Harrati A, Sadik C, Ouammou M, et al. New low-cost ceramic microfiltration membrane made from natural magnesite for industrial wastewater treatment. *J Environ Chem Eng*. 2020;8(4):103906. <http://doi.org/10.1016/j.jece.2020.103906>.
  49. Mohamed M, Dayirou N, Mohamed H, André N, Gisèle Laure L-N, Daniel N. Effect of porogenic agent type and firing temperatures on properties of low-cost microfiltration membranes

- from kaolin. *Trans Indian Ceram Soc.* 2020;79(1):1-12. <http://doi.org/10.1080/0371750X.2019.1692695>.
50. Dong Y, Feng X, Dong D, Wang S, Yang J, Gao J, et al. Elaboration and chemical corrosion resistance of tubular macro-porous cordierite ceramic membrane supports. *J Membr Sci.* 2007;304(1-2):65-75. <http://doi.org/10.1016/j.memsci.2007.06.058>.
51. Najmi H, El-Tabach E, Chetehouna K, Gascoin N, Falempin F. Effect of flow configuration on Darcian and Forchheimer permeabilities determination in a porous composite tube. *Int J Hydrogen Energy.* 2016;41(1):316-23. <http://doi.org/10.1016/j.ijhydene.2015.10.054>.
52. Lagdali S, Miyah Y, El-Habacha M, Mahmoudy G, Benjelloun M, Iaich S, et al. Performance assessment of a phengite clay-based flat membrane for microfiltration of real-wastewater from clothes washing: characterization, cost estimation, and regeneration. *Case Stud Chem Environ Eng.* 2023;8:100388. <http://doi.org/10.1016/j.cscee.2023.100388>.
53. Alsubei MD, Reid B, Aljlil SA, Coppens MO, Campos LC. Fabrication and characterization of coated ceramic membranes from natural sources for water treatment applications. *J Membr Sci.* 2024;690:122226. <http://doi.org/10.1016/j.memsci.2023.122226>.
54. Gautam S, Cole DR. Effects of pore connectivity and tortuosity on the dynamics of fluids confined in sub-nanometer pores. *Phys Chem Chem Phys.* 2022;24(19):11836-47. <http://doi.org/10.1039/D1CP04955K>.
55. Edition F. Guidelines for drinking-water quality. *WHO Chron.* 2011;38(4):104-8.